Supplementary Information

Table S1. CMIP6 models.

ESM	Reference	Land model	N cycle	DGVM	Fire	Soil depth (m)*
ACCESS-ESM1-5	Ziehn et al. 2020[38]	CABLE2.4 with CASA-CNP	Yes (& P)	No	No	2.9
CanESM5	Swart et al. 2019[39]	CLASS3.6-CTEM1.2	No	No	No	4.1
CESM2	Danabasoglu et al. 2020[40]	CLM5	Yes	No	Yes	8
CMCC-ESM2	Lovato et al. 2022[41]	CLM4.5	Yes	No	Yes	35.2
CNRM-ESM2-1	Séférian et al. 2019[42]	ISBA-CTRIP	No, implicit	No	Yes	10
GFDL-ESM4	Dunne et al. 2020[43]	GFDL-LM4.1	No	Yes	Yes	8.8
IPSL-CM6A-LR	Boucher et al. 2020[44]	ORCHIDEE, branch 2.0	No, implicit	No	No	2
MIROC-ES2L	Hajima et al. 2020[45]	MATSIRO VISIT-e	Yes	No	No	14
MPI-ESM1-2-LR	Müller et al. 2018[46]	JSBACH3.2	Yes	Yes	Yes	9.8
MRI-ESM2-0	Yukimoto et al. 2019[47]	HAL	No	No	Yes	10
NorESM2-LM	Seland et al. 2020[48]	CLM5	Yes	No	Yes	9
UKESM1-0-LL	Sellar et al. 2019[49]	JULES-ES-1.0	Yes	Yes	No	3

* Soil depth at the middle of the bottom layer, reported in the model

Table S2. CMIP6 ESMs and variant labels in each experiment.

	ESM	piControl	1pctCO2	ssp585	1pctCO2-bgc	ssp585-bgc
1	ACCESS-ESM1-5	r1i1p1f1	r1i1p1f1	r1i1p1f1	r1i1p1f1	r1i1p1f1
2	CanESM5	r1i1p1f1, r1i1p2f1	r1i1p1f1	r1i1p2f1	r1i1p1f1	r1i1p2f1
3	CESM2	r1i1p1f1	r1i1p1f1	r1i1p1f1	r1i1p1f1	-
4	CMCC-ESM2	r1i1p1f1	r1i1p1f1	r1i1p1f1	r1i1p1f1	-
5	CNRM-ESM2-1	r1i1p1f2	r1i1p1f2	r1i1p1f2	r1i1p1f2	r1i1p1f2
6	GFDL-ESM4	r1i1p1f1	r1i1p1f1	r1i1p1f1	r1i1p1f1	-
7	IPSL-CM6A-LR	r1i1p1f1	r1i1p1f1	r1i1p1f1	r1i1p1f1	r1i1p1f1
8	MIROC-ES2L	r1i1p1f2	r1i1p1f2	r1i1p1f2	r1i1p1f2	r1i1p1f2
9	MPI-ESM1-2-LR	r1i1p1f1	r1i1p1f1	r1i1p1f1	r1i1p1f1	-
10	MRI-ESM2-0	r1i2p1f1	r1i2p1f1	r1i2p1f1	r1i2p1f1	r1i1p1f1
11	NorESM2-LM	r1i1p1f1	r1i1p1f1	r1i1p1f1	r1i1p1f1	r1i1p1f1
12	UKESM1-0-LL	r1i1p1f2	r1i1p1f2	r1i1p1f2	r1i1p1f2	r4i1p1f2

Table S3. Mean values and constrained 17–83% and 5–95% ranges of the future changes in surface climate and climate-driven carbon cycle estimated by the CMIP6 ESMs. The emergent constraint is estimated for the 120–139 year means of 1pctCO2 and 2072–2091 year means of SSP5-8.5 that both correspond to intermodel mean 4.4 °C warming relative to preindustrial level.

						Climate-driven		
		ΔT_{ft} (°C)	ΔSM_{ft} (%)	ΔP_{ft} (%)	ΔRAD_{ft} (%)	ΔGPP_{ft} (%)	ΔNPP_{ft} (%)	ΔNEP_{ft} (GtC year^{-1})
Original	Mean	5.8	-11.8	-16.1	3.0	-27.8	-47.4	-0.27
	5th	2.7	-26.6	-37.7	-0.7	-67.9	-121.3	-0.59
	17th	4.2	-20.2	-28.5	0.9	-50.7	-89.8	-0.46
	83rd	7.6	-3.3	-3.7	5.2	-4.8	-5.0	-0.09
	95th	9.0	3.1	5.6	6.8	12.4	26.6	0.05
Constrained	Mean	4.7	-5.7	-7.0	2.0	-11.5	-21.1	-0.16
	5th	2.2	-16.8	-22.7	-1.4	-41.7	-81.4	-0.42
	17th	3.3	-12.1	-16.0	0.0	-28.8	-55.6	-0.31
	83rd	6.2	0.7	2.1	3.9	5.8	13.5	-0.01
	95th	7.2	5.4	8.8	5.3	18.7	39.2	0.10
Relative reductions in variance (%)		34.5	44.0	46.7	21.9	43.3	33.5	33.8

Table S4. Mean values and constrained 17–83% and 5–95% ranges of the future changes in surface climate and climate-driven carbon cycle. The emergent constraint is estimated for the 61–80 year means of 1pctCO2 and 2031–2050 year means of SSP5-8.5 that both correspond to intermodel mean 2.0 °C warming relative to preindustrial level.

						Climate-driven		
		ΔT_{ft} (°C)	ΔSM_{ft} (%)	ΔP_{ft} (%)	ΔRAD_{ft} (%)	ΔGPP_{ft} (%)	ΔNPP_{ft} (%)	ΔNEP_{ft} (GtC year^{-1})
Original	Mean	2.6	-6.2	-7.5	1.5	-11.5	-18.5	-0.13
	5th	0.9	-16.7	-22.6	-1.3	-29.0	-48.8	-0.34
	17th	1.6	-12.2	-16.1	-0.1	-21.6	-35.9	-0.25
	83rd	3.5	-0.1	1.2	3.2	-1.5	-1.1	0.00
	95th	4.3	4.4	7.6	4.4	6.0	11.8	0.09
Constrained	Mean	2.0	-2.6	-1.5	0.5	-3.9	-7.8	-0.07
	5th	0.7	-11.3	-13.1	-1.8	-16.3	-32.6	-0.26
	17th	1.2	-7.6	-8.2	-0.8	-11.0	-22.0	-0.17
	83rd	2.7	2.5	5.1	1.9	3.2	6.4	0.04
	95th	3.2	6.2	10.1	2.9	8.4	17.0	0.12
Relative reductions in variance (%)		39.7	30.7	41.0	31.5	50.0	33.0	21.1

Table S5. Mean values and constrained 17–83% and 5–95% ranges of the future changes in surface climate and climate-driven carbon cycle. The emergent constraint is estimated for the 61–80 year means of 1pctCO2 and 2031–2050 year means of SSP5-8.5 that both correspond to intermodel mean 4.0 °C warming relative to preindustrial level.

		ΔT_{ft} (°C)	ΔSM_{ft} (%)	ΔP_{ft} (%)	ΔRAD_{ft} (%)	Climate-driven ΔGPP_{ft} (%)	ΔNPP_{ft} (%)	ΔNEP_{ft} (GtC year^{-1})
Original	Mean	5.4	-11.0	-14.8	2.9	-24.5	-42.2	-0.26
	5th	2.5	-25.1	-35.2	-0.5	-61.4	-108.0	-0.56
	17th	3.7	-19.1	-26.5	0.9	-45.7	-79.9	-0.44
	83rd	7.0	-2.9	-3.2	4.8	-3.4	-4.5	-0.09
	95th	8.3	3.1	5.5	6.3	12.3	23.6	0.04
Constrained	Mean	4.3	-5.6	-6.8	1.9	-9.5	-18.8	-0.16
	5th	2.0	-16.5	-22.3	-1.1	-37.1	-72.5	-0.41
	17th	3.0	-11.8	-15.7	0.2	-25.1	-49.6	-0.31
	83rd	5.7	0.7	2.1	3.6	6.3	11.9	-0.01
	95th	6.7	5.4	8.8	4.9	18.1	34.9	0.09
Relative reductions in variance (%)		34.6	39.5	41.7	21.2	44.0	33.4	29.4

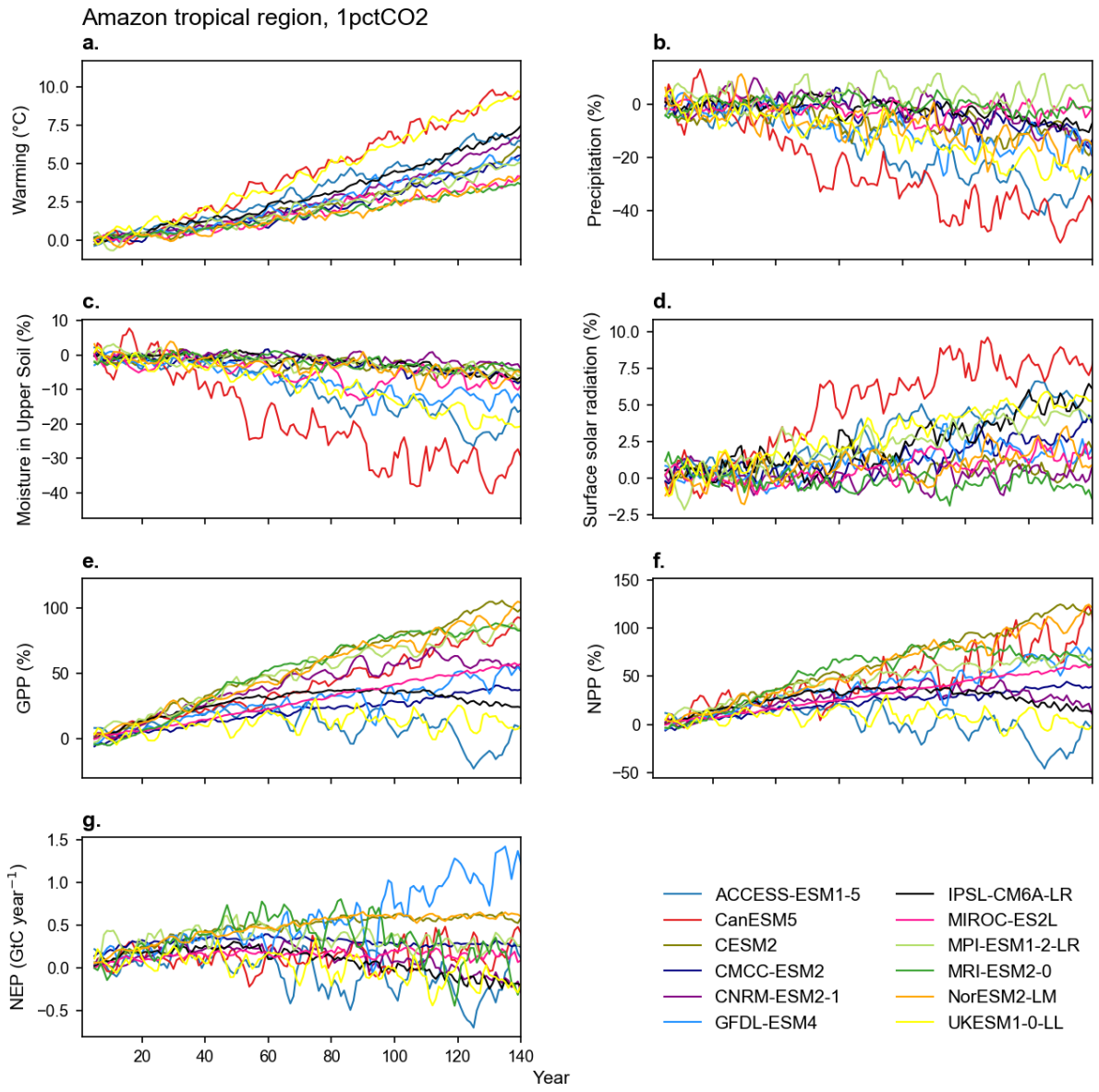

Fig. S1. Time series of surface climate and carbon cycle over the Amazon forest region estimated by CMIP6 ESMs under the 1pctCO2 scenario.

Five-year moving averages of **(a)** ΔT (°C), **(b)** ΔP (%), **(c)** ΔSM, **(d)** ΔRAD (%), **(e)** ΔGPP (%), **(f)** ΔNPP (%), and **(g)** ΔNEP (GtC year^{-1}) estimates are shown.

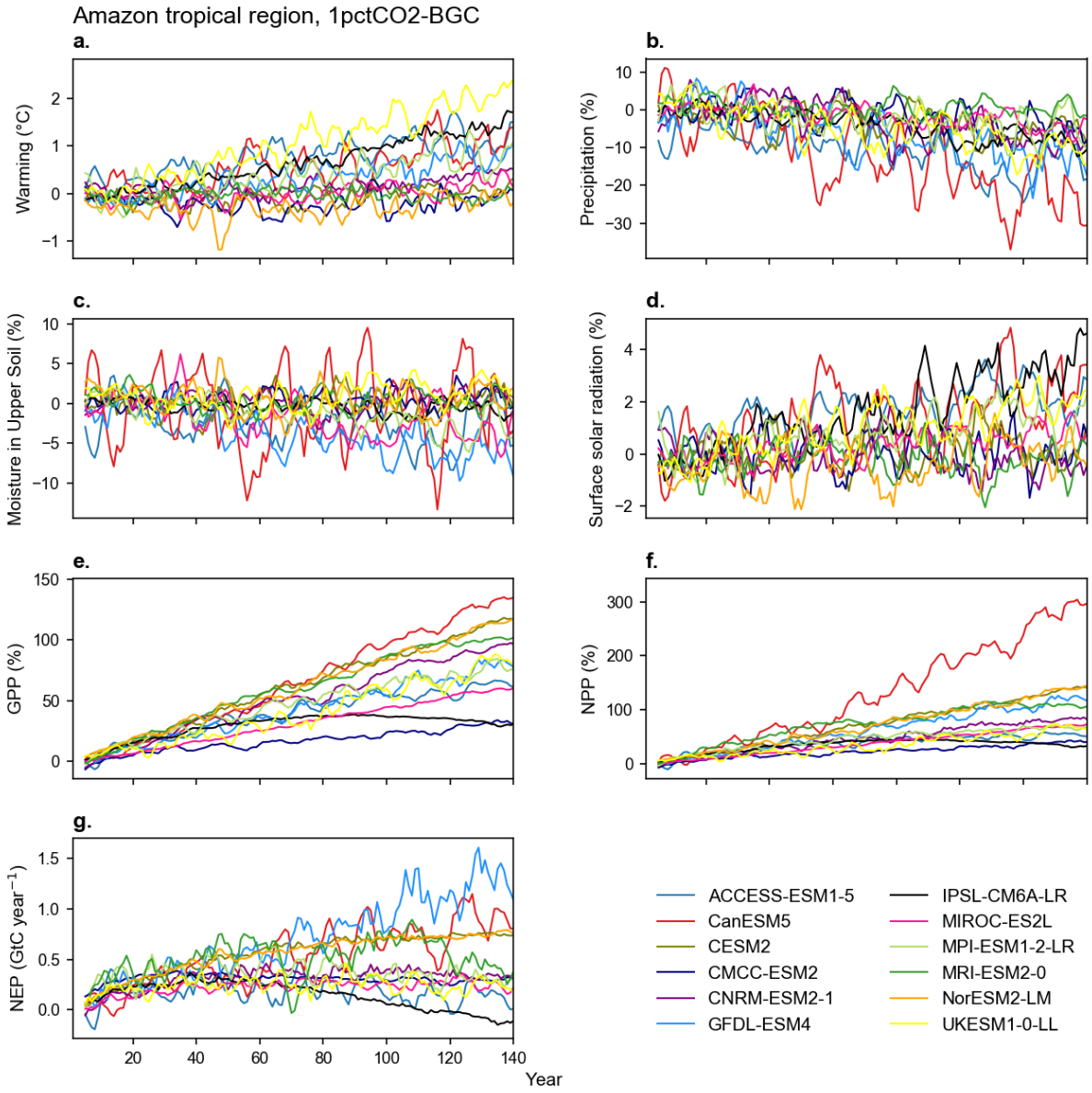

Fig. S2. Time series of surface climate and carbon cycle over the Amazon forest region estimated by CMIP6 ESMs under the 1pctCO2-BGC scenario.

Five-year moving averages of **(a)** ΔT (°C), **(b)** ΔP (%), **(c)** ΔSM, **(d)** ΔRAD (%), **(e)** ΔGPP (%), **(f)** ΔNPP (%), and **(g)** ΔNEP (GtC year^{-1}) estimates are shown.

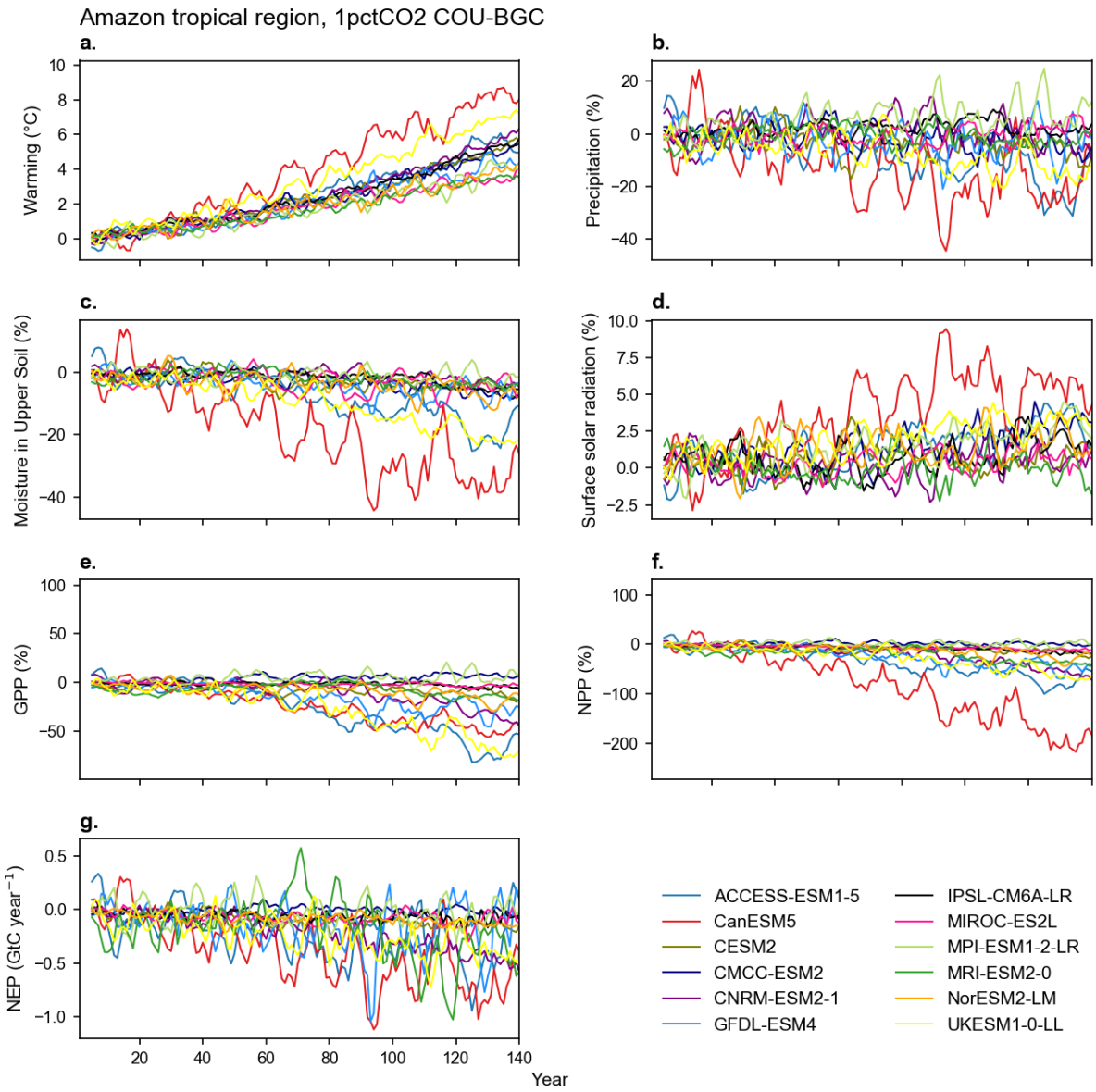

Fig. S3. Time series of changes driven by the radiative impact of CO_2 concentration on surface climate and carbon cycle over the Amazon forest region estimated by CMIP6 ESMs under the 1pctCO2 scenario.

Five-year moving averages of **(a)** ΔT (°C), **(b)** ΔP (%), **(c)** ΔSM, **(d)** ΔRAD (%), **(e)** ΔGPP (%), **(f)** ΔNPP (%), and **(g)** ΔNEP (GtC year^{-1}) estimates are shown. Climate-driven changes (changes driven by the radiative impact of CO_2 concentration) are estimated as the difference between the 1pctCO2 and 1pctCO2-BGC scenarios.

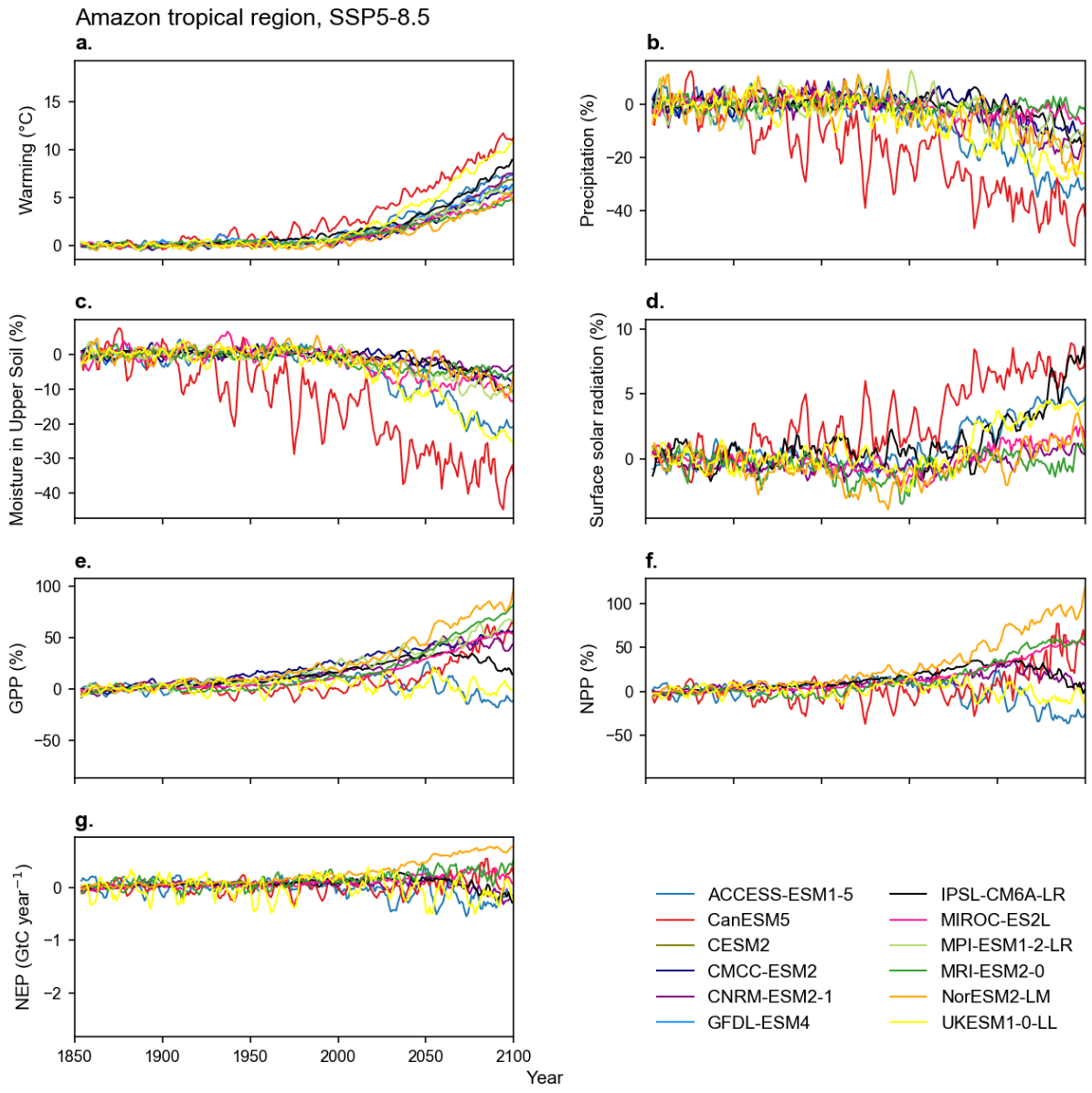

Fig. S4. Time series of surface climate and carbon cycle over the Amazon forest region estimated by CMIP6 ESMs under the SSP5-8.5 scenario.

Five-year moving averages of **(a)** ΔT (°C), **(b)** ΔP (%), **(c)** ΔSM, **(d)** ΔRAD (%), **(e)** ΔGPP (%), **(f)** ΔNPP (%), and **(g)** ΔNEP (GtC year^{-1}) estimates are shown.

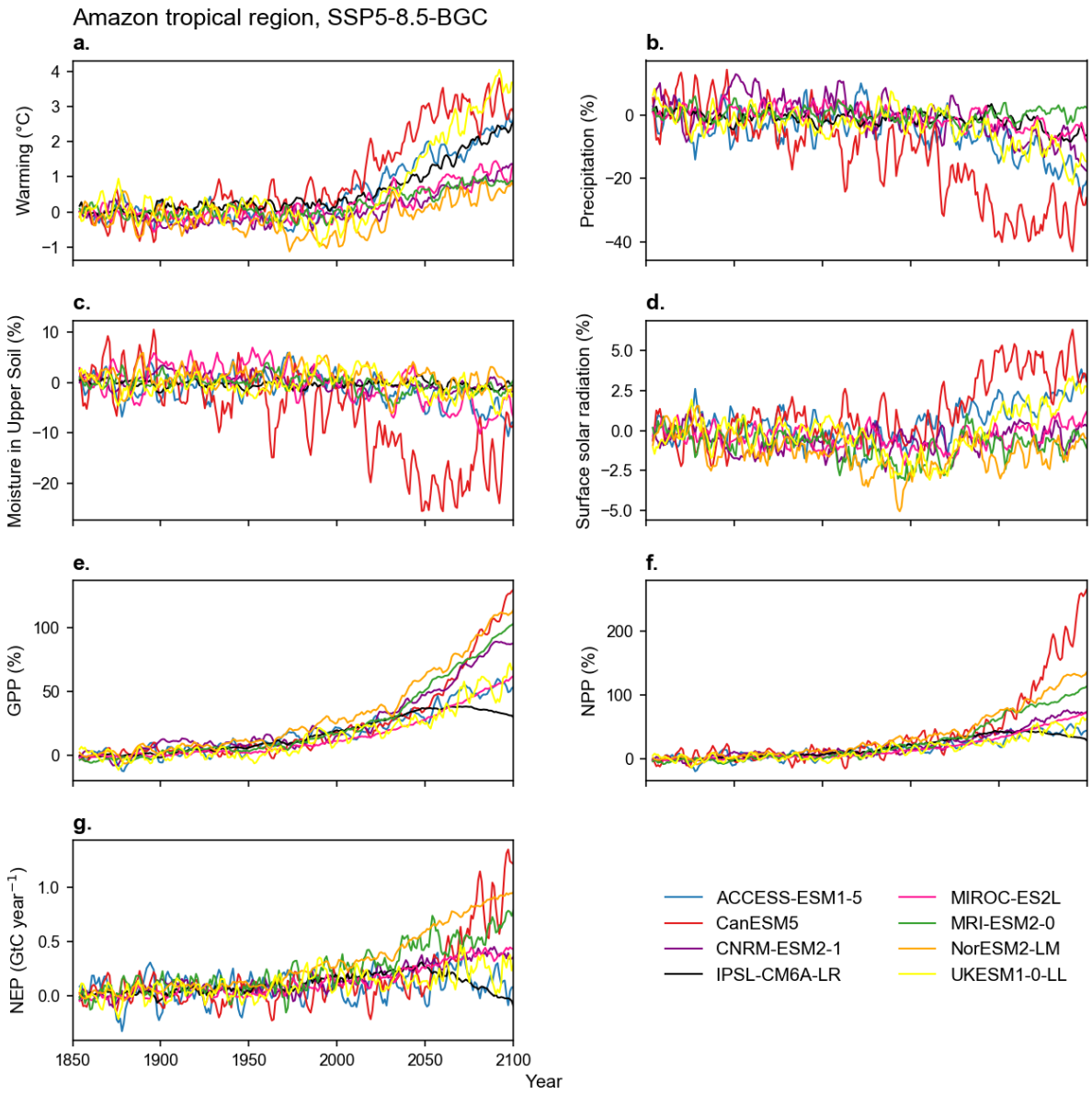

Fig. S5. Time series of surface climate and carbon cycle over the Amazon forest region estimated by the CMIP6 ESMs under the SSP5-8.5-BGC scenario.

Five-year moving averages of **(a)** ΔT (°C), **(b)** ΔP (%), **(c)** ΔSM, **(d)** ΔRAD (%), **(e)** ΔGPP (%), **(f)** ΔNPP (%), and **(g)** ΔNEP (GtC year^{-1}) estimates are shown.

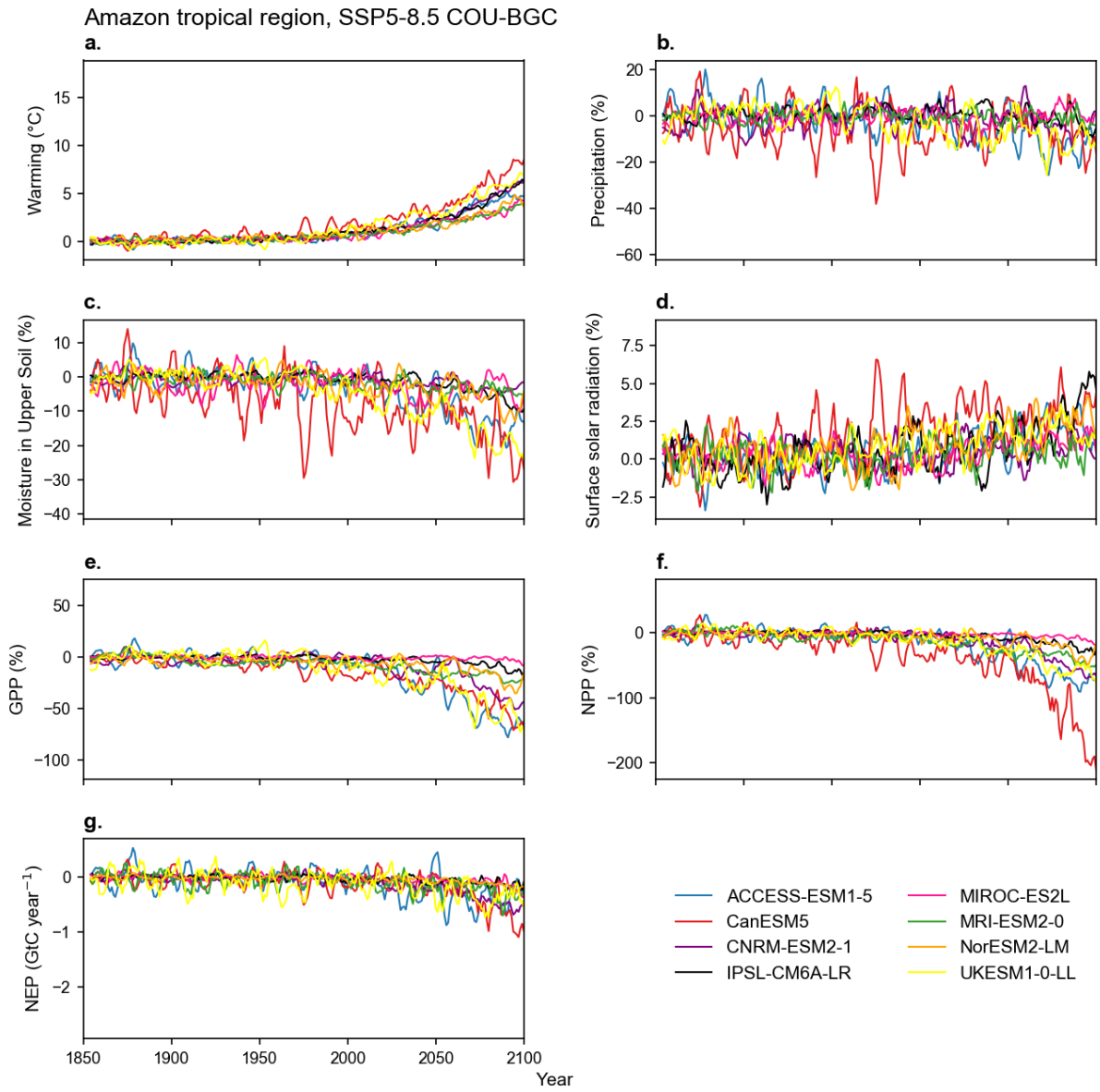

Fig. S6. Time series of changes driven by the radiative impact of CO_2 concentration on the surface climate and carbon cycle over the Amazon forest region estimated by the CMIP6 ESMs under the SSP5-8.5 scenario.

Five-year moving averages of **(a)** ΔT (°C), **(b)** ΔP (%), **(c)** ΔSM, **(d)** ΔRAD (%), **(e)** ΔGPP (%), **(f)** ΔNPP (%), and **(g)** ΔNEP (GtC year^{-1}) estimates are shown. Climate-driven changes (changes driven by the radiative impact of CO_2 concentration) are estimated as the difference between the SSP5-8.5 and SSP5-8.5-BGC scenarios.

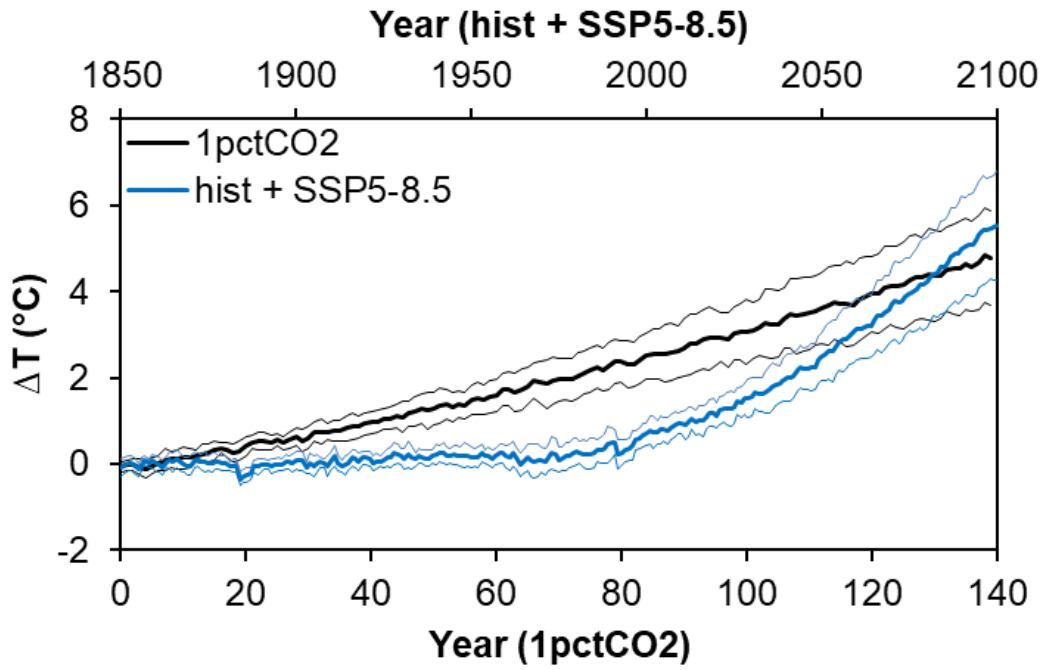

Fig. S7. Time series of ensemble mean estimates of ΔT ± one standard deviation of twelve CMIP6 ESMs.

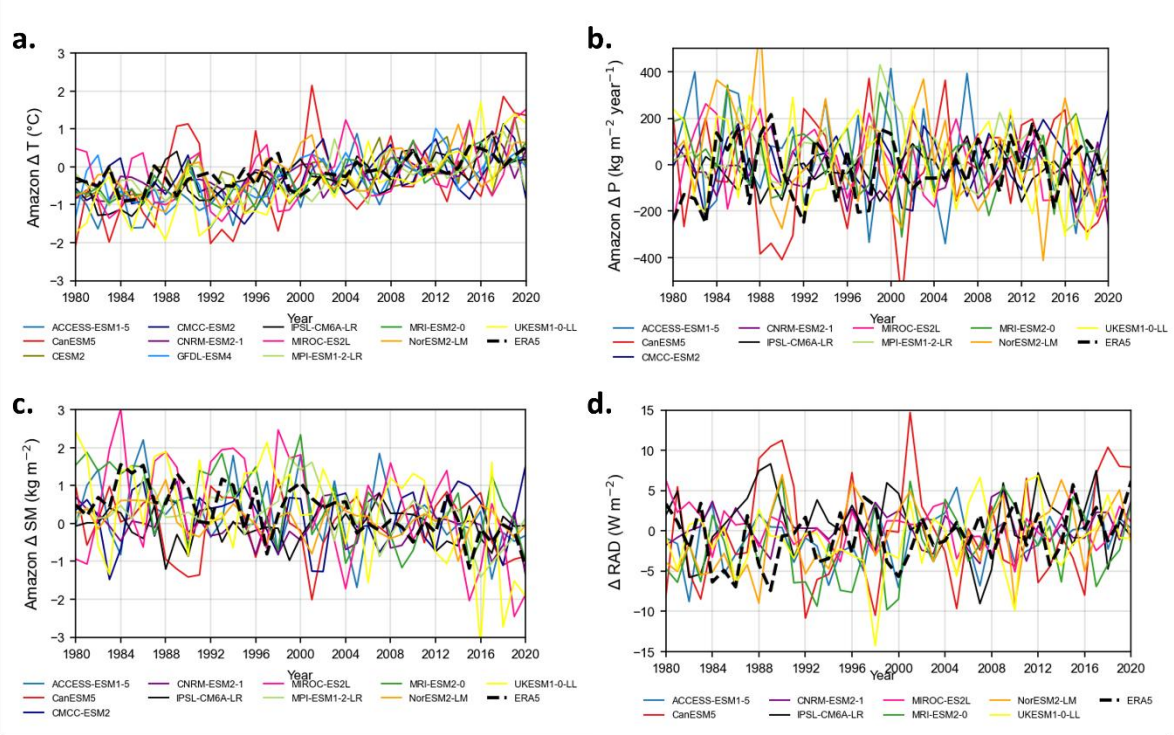

Fig. S8. Evaluation of CMIP6 ESM estimates of climate variables over the Amazon forest region against the ERA5 reanalysis dataset.

Anomalies of **(a)** ΔT (°C), **(b)** ΔP (kg m^{-2} year^{-1}), **(c)** Δ SM (kg m^{-2}) and **(d)** Δ RAD (W m^{-2}) relative to the 2000–2018 mean are shown.

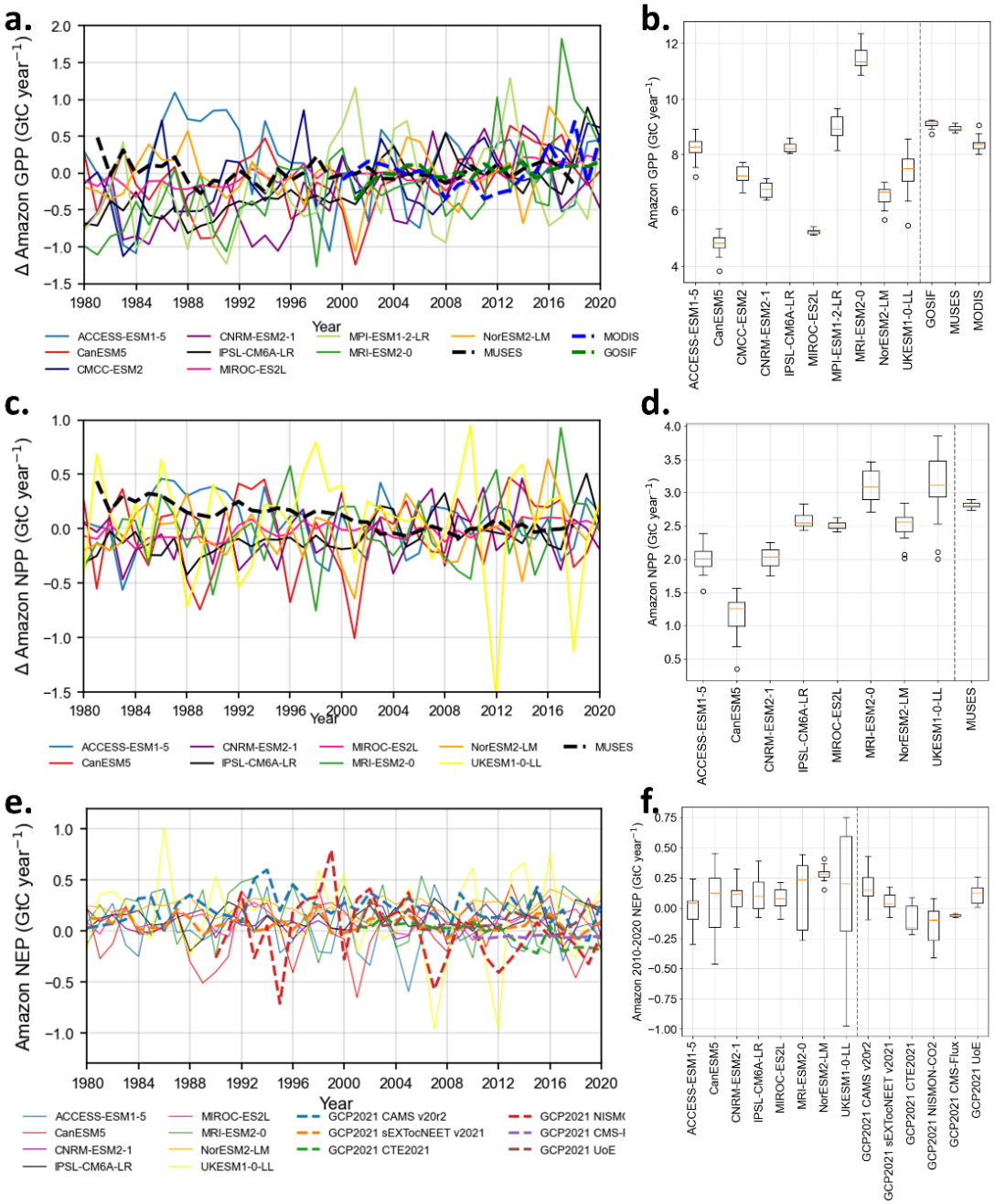

Fig. S9. Evaluation of CMIP6 ESM estimates of carbon fluxes over the Amazon forest region against historical datasets.

Anomalies are shown for **(a)** GPP (GtC year^{-1}) and **(c)** NPP (GtC year^{-1}) relative to the 2000–2018 mean, and absolute values are shown for **(e)** NEP (GtC year^{-1}). The box plots for absolute **(b)** GPP and **(d)** NPP estimates over 2000–2018 and **(f)** NEP over 2010–2020 extend from the first quartile to the third quartile of the time series data, with an orange line at the median. The whiskers extend from the box by 1.5 times the interquartile range (data points outside the range are considered outliers).

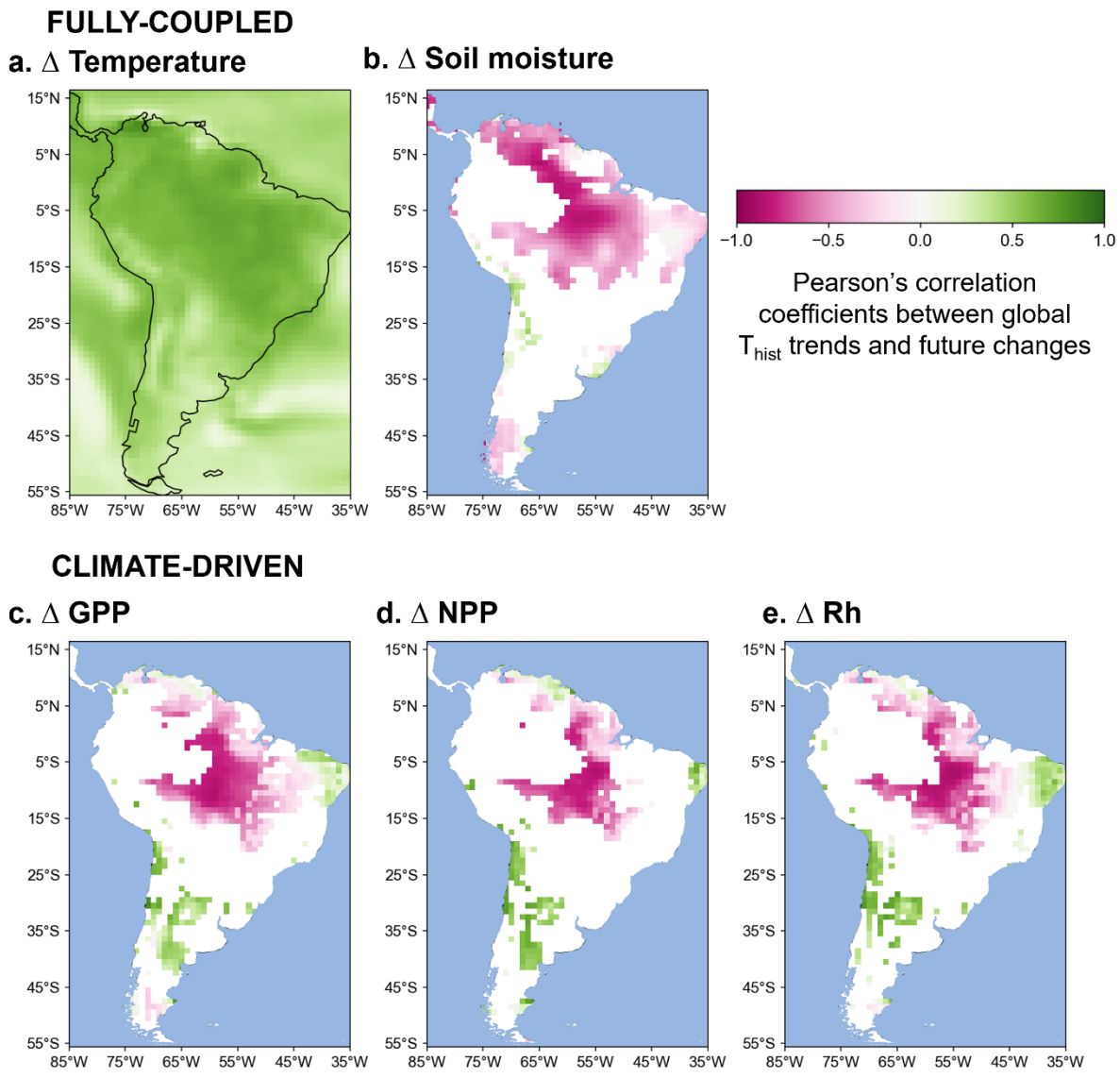

Fig. S10. Spatial patterns of inter-model Pearson's correlation coefficients between the past 1980–2014 temperature trend and future changes in surface climate and carbon cycle.

Spatial patterns of inter-model Pearson's correlation coefficients between the past 1980–2014 global T_{hist} trend and future changes in **(a)** ΔT_{ft} and **(b)** ΔSM and climate change-driven changes in **(c)** ΔGPP_{ft}, **(d)** ΔNPP_{ft}, and **(e)** ΔRh_{ft} estimated from the difference between coupled (COU) and biogeochemically coupled (BGC) simulations. We drew only the correlations that are significant ($p < 0.1$ based on Welch's t test). Here, N=20 (SSP5-8.5 by 8 models and 1pctCO2 by 12 models).

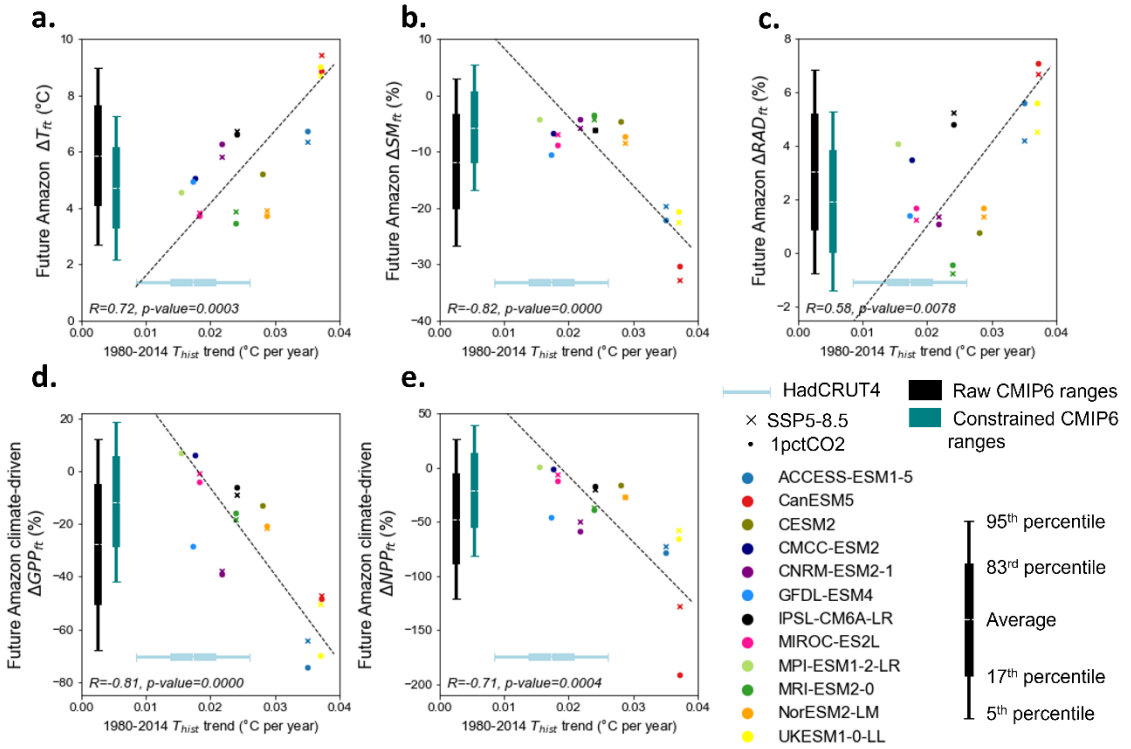

Fig. S11. Observational constraints on the future climate and climate-driven changes in the carbon cycle over the Amazon forest region estimated by the CMIP6 ESMs.

The vertical axes indicate the future **(a)** ΔT (°C), **(b)** ΔTSM (°C), ΔRAD (°C) and climate-driven changes in **(d)** GPP (%) and **(e)** NPP (%) over the Amazon forest region. The horizontal axes show the past global (1980–2014) trends of T_{hist} (°C year^{-1}). Pearson's correlation coefficients and p-values for two scenarios combined (SSP5-8.5 and 1pctCO2) are denoted at the bottom of the panels. The black dashed lines show the linear reduced major axis regressions. The horizontal box plots indicate the mean (white line), 17–83% range (box) and 5–95% range (horizontal bar) of HadCRUT4[34] estimated by ref. [7] (light blue). The vertical box plots show the same as the horizontal box plots but for the raw CMIP6 ESMs (black) and the constrained ranges using the observations (teal). The emergent constraint is estimated for the 120–139 year means of 1pctCO2 and 2072–2091 year means of SSP5-8.5 that both correspond to intermodel mean 4.4 °C warming relative to preindustrial level.

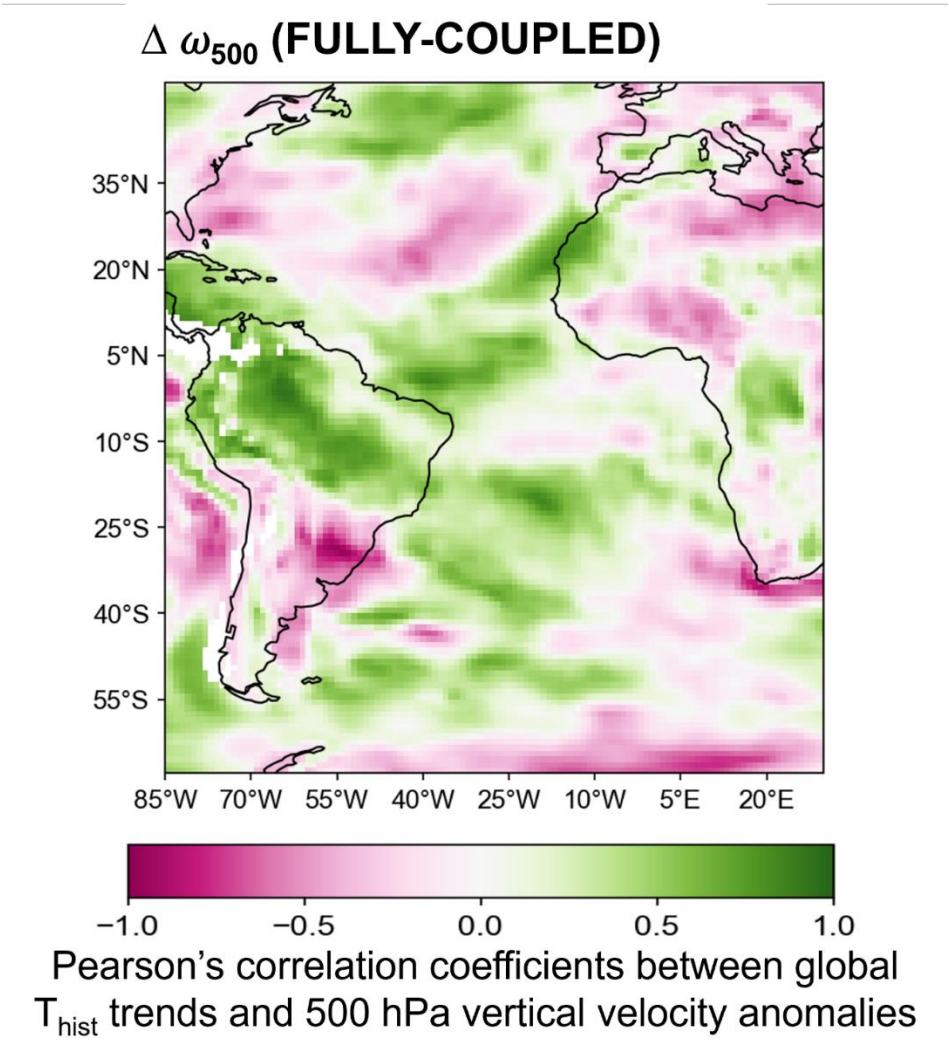

Fig. S12. Spatial patterns of inter-model Pearson's correlation coefficients between the past 1980–2014 T_{hist} trend and future changes in 500 hPa vertical velocity.

Spatial patterns of inter-model Pearson's correlation coefficients between the 1980–2014 global T_{hist} trend and future changes in 500 hPa vertical velocity (omega-500, Pa s^{-1}, $\Delta\omega_{500}$) in fully coupled simulation. We drew only the correlations that are significant ($p < 0.1$ based on Welch's t test). Here, N=15 (SSP5-8.5 by 5 models and 1pctCO2 by 10 models, reduced number because some model data were not available).

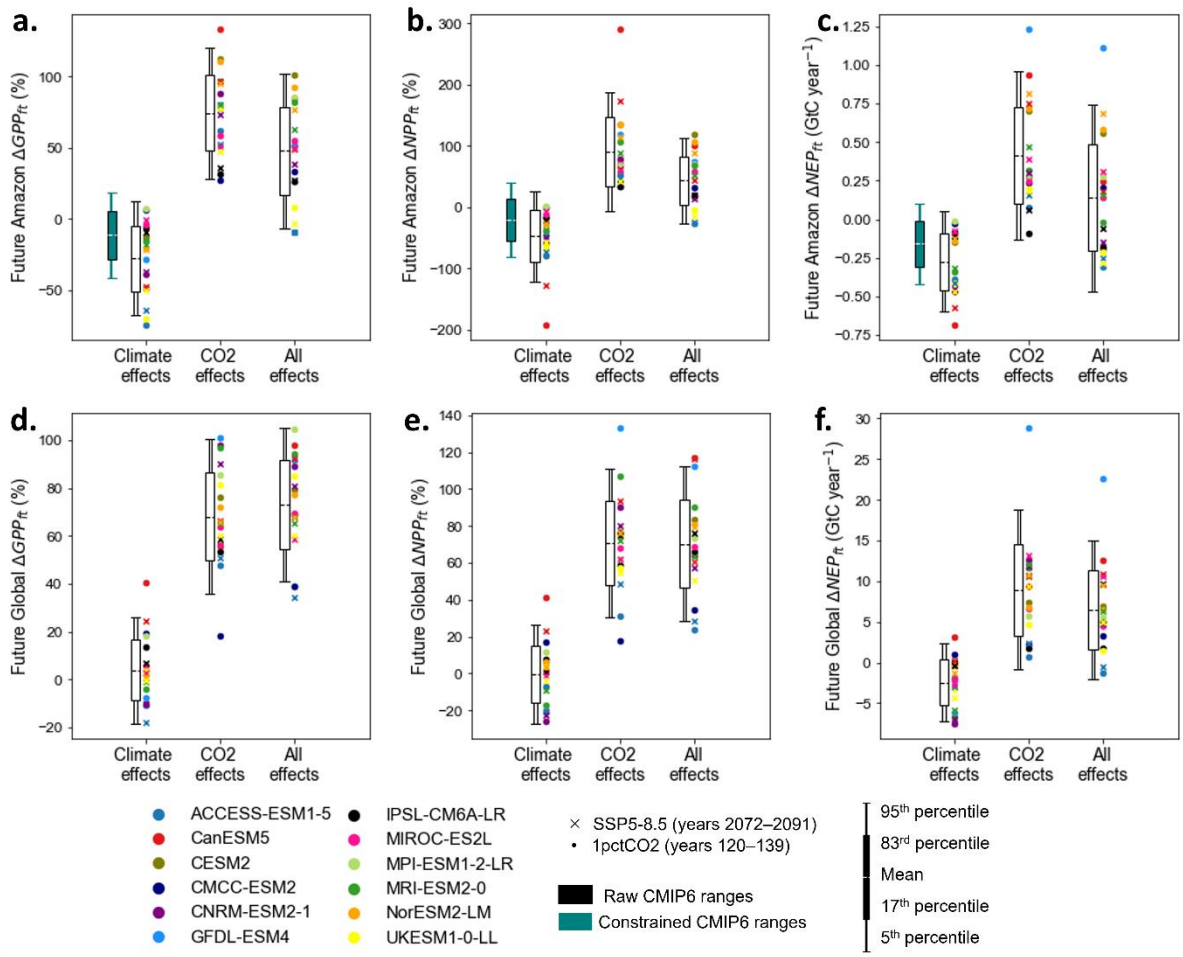

Fig. S13. Uncertainty range for the CMIP6 ESM estimates of future changes in carbon fluxes globally and over the Amazon forest region.

Box plots show inter-model ranges and dots show individual model estimates of future changes in **(a-c)** Amazon and **(d-e)** global (**a, d**) ΔGPP (%), (**b, e**) ΔNPP (%) and (**c, f**) Δ NEP (GtC year^{-1}) for the 120–139 year means of 1pctCO2 and 2072–2091 year means of SSP5-8.5 that both correspond to intermodel mean 4.4 °C warming relative to preindustrial level. Climate effects indicate future climate-induced changes, estimated using COU-BGC experiments, CO2 effects indicate CO_2 fertilisation-induced changes, estimated using BGC experiments, and all effects indicate total changes, estimated using COU experiments. The vertical box plots indicate the mean (white line), 17–83% range (box) and 5–95% range (horizontal bar) of the raw CMIP6 ESMs (black) and the constrained ranges using the observations (teal).

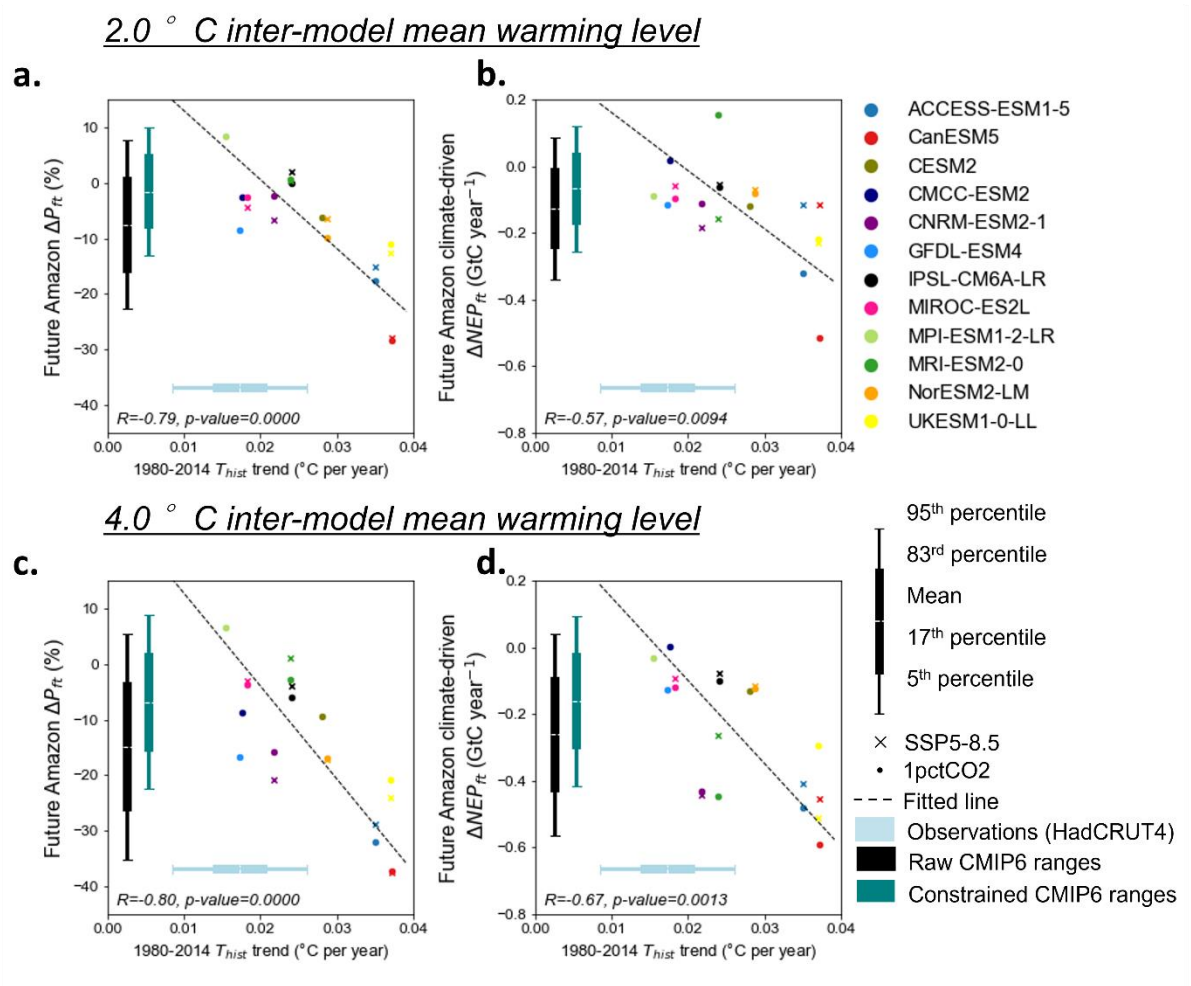

Fig. S14. Observational constraints on the future surface climate and climate-driven changes in carbon cycle in the Amazon forest region.

Same as Fig. 2 but for mean inter-model warming levels of **(a, b)** 2 °C and **(c, d)** 4.0 °C relative to preindustrial level. The vertical axes indicate the **(a, c)** ΔP_{ft} (%) and **(b, d)** climate-driven ΔNEP_{ft} (GtC year^{-1}) in the Amazon forest estimated by the CMIP6 ESMs. The horizontal axes show the past global (1980–2014) trends of T_{hist} (°C year^{-1}). Pearson's correlation coefficients and p-values for two scenarios combined (SSP5-8.5 and 1pctCO2) are denoted at the bottom of the panels. The black dashed lines show the linear reduced major axis regressions. The horizontal box plots indicate the mean (white line), 17–83% range (box) and 5–95% range (horizontal bar) of HadCRUT4[31] estimated by ref. [7] (light blue). The vertical box plots show the same as the horizontal box plots but for the raw CMIP6 ESMs (black) and the constrained ranges using the observations (teal). The emergent constraint is estimated for the **(a, b)** 61–80 year means of 1pctCO2 and 2031–2050 year means of SSP5-8.5, and **(c, d)** 112–131 year means of 1pctCO2 and 2067–2086 year means of SSP5-8.5.

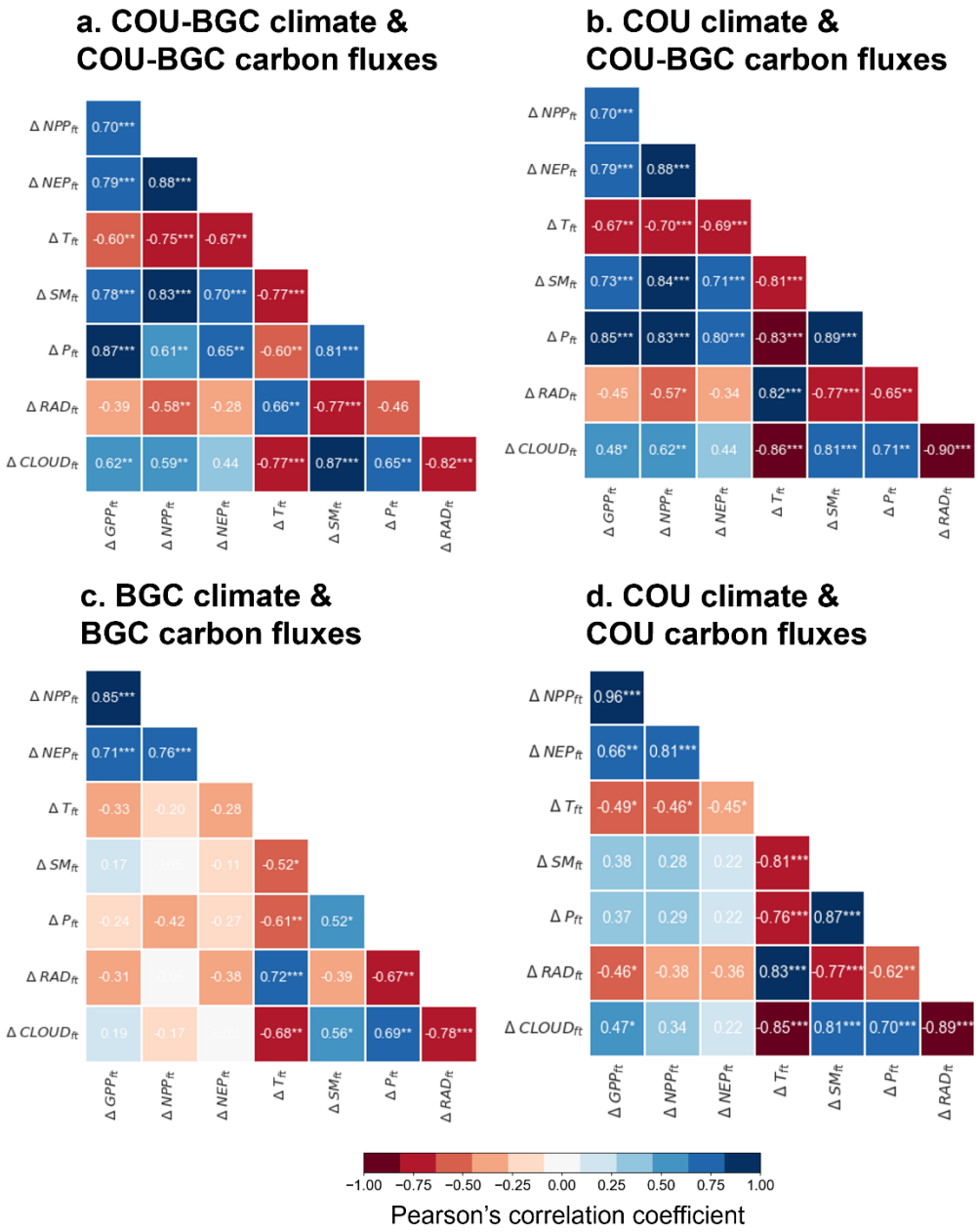

Fig. S15. Inter-model Pearson's correlation between future changes in surface climate and carbon cycle in the Amazon forest.

The heatmaps show Pearson's correlation coefficients between future regional changes in surface climate variables, including ΔT (°C), ΔP (%) and Δ SM (%), ΔRAD (%), total cloud cover (%), and carbon fluxes, including ΔGPP (%), ΔNPP (%), and Δ NEP (GtC year^{-1}), in the Amazon forest estimated by the CMIP6 ESMs for two scenarios, 1pctCO2 and SSP5-8.5. The correlation coefficients are estimated for **(a)** the COU-BGC climate and COU-BGC carbon fluxes, **(b)** COU climate and COU-BGC carbon fluxes, **(c)** BGC climate and BGC carbon fluxes, and **(d)** COU climate and COU carbon fluxes. The COU setup includes all effects, COU-BGC includes CO_2 radiative effects, and BGC includes CO_2 physiological, non-CO_2 and land-use change effects on climate. COU climate and COU carbon fluxes. The COU setup includes all effects, COU-BGC includes climate impacts, and BGC includes CO_2 fertilization effects on carbon cycle. The statistical significance is shown by asterisks (* for p value < 0.05, ** for p value < 0.01, and *** for p value < 0.001).

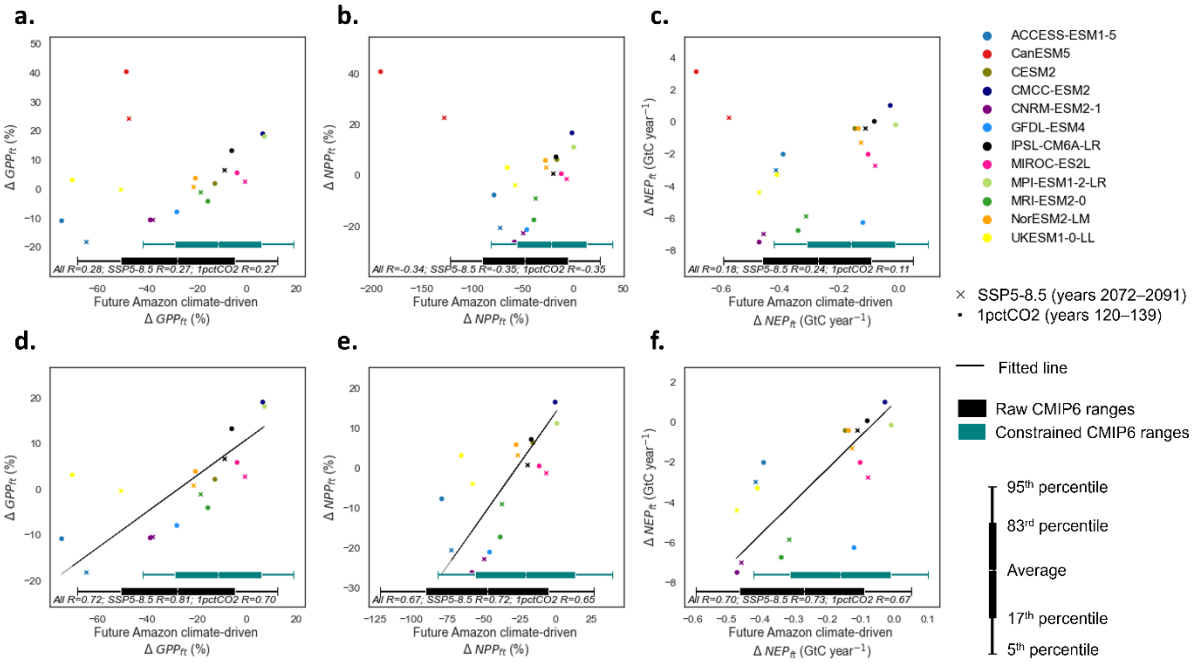

Fig. S16. Inter-model correlations between climate-driven changes in the future Amazon and global (**a, d**) ΔGPP (%), (**b, e**) ΔNPP (%) and (**c, f**) Δ NEP (GtC year^{-1}).

Panels **a, b, c** show data and correlations for all considered models, and panels (**d, e, f**) show data and correlations for all models excluding CanESM5. The correlations are significant at the 5% level. The black lines show the linear regressions for two experiments, SSP5-8.5 and 1pctCO2, combined. The horizontal boxplots show the average (white line), 17–83% range (box) and 5–95% range (vertical bar) for the raw CMIP6 ESMs (black) and the constrained ranges using the observations (teal).

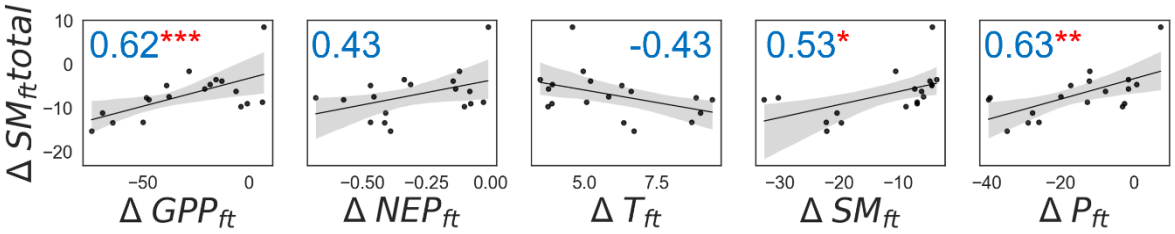

Fig. S17. Inter-model correlation analysis of future changes in surface climate and climate-driven carbon cycle in the Amazon forest (addition to Fig. 3).

The matrix shows scatterplots, fitted linear regression lines (black lines) with 95% bootstrap confidence interval (grey shading), and Pearson's correlation coefficients between future regional changes in climate variables, including ΔT_{ft} (°C), ΔP_{ft} (%) and ΔSM_{ft} (%), total ΔSM_{ft} (%) and climate-driven changes in carbon fluxes, including ΔGPP_{ft} (%), and ΔNEP_{ft} (GtC year^{-1}), in the Amazon forest estimated by the CMIP6 ESMs for two scenarios, 1pctCO2 and SSP5-8.5. The statistical significance is shown by asterisks (** for p value < 0.01 and *** for p value < 0.001).

References

38. Ziehn, T. *et al.* The Australian Earth System Model: ACCESS-ESM1.5. *JSHESS* **70**, 193–214 (2020).
39. Swart, N. C. *et al.* The Canadian Earth System Model version 5 (CanESM5.0.3). *Geoscientific Model Development* **12**, 4823–4873 (2019).
40. Danabasoglu, G. *et al.* The Community Earth System Model Version 2 (CESM2). *Journal of Advances in Modeling Earth Systems* **12**, e2019MS001916 (2020).
41. Lovato, T. *et al.* CMIP6 Simulations With the CMCC Earth System Model (CMCC-ESM2). *Journal of Advances in Modeling Earth Systems* **14**, e2021MS002814 (2022).
42. Séférian, R. *et al.* Evaluation of CNRM Earth System Model, CNRM-ESM2-1: Role of Earth System Processes in Present-Day and Future Climate. *Journal of Advances in Modeling Earth Systems* **11**, 4182–4227 (2019).
43. Dunne, J. P. *et al.* The GFDL Earth System Model Version 4.1 (GFDL-ESM 4.1): Overall Coupled Model Description and Simulation Characteristics. *Journal of Advances in Modeling Earth Systems* **12**, e2019MS002015 (2020).
44. Boucher, O. *et al.* Presentation and Evaluation of the IPSL-CM6A-LR Climate Model. *Journal of Advances in Modeling Earth Systems* **12**, e2019MS002010 (2020).
45. Hajima, T. *et al.* Development of the MIROC-ES2L Earth system model and

the evaluation of biogeochemical processes and feedbacks. *Geoscientific Model Development* **13**, 2197–2244 (2020).

46. Müller, W. A. *et al.* A Higher-resolution Version of the Max Planck Institute Earth System Model (MPI-ESM1.2-HR). *Journal of Advances in Modeling Earth Systems* **10**, 1383–1413 (2018).
47. Yukimoto, S. *et al.* The Meteorological Research Institute Earth System Model Version 2.0, MRI-ESM2.0: Description and Basic Evaluation of the Physical Component. *Journal of the Meteorological Society of Japan. Ser. II* **advpub**, (2019).
48. Seland, Ø. *et al.* Overview of the Norwegian Earth System Model (NorESM2) and key climate response of CMIP6 DECK, historical, and scenario simulations. *Geoscientific Model Development* **13**, 6165–6200 (2020).
49. Sellar, A. A. *et al.* UKESM1: Description and Evaluation of the U.K. Earth System Model. *Journal of Advances in Modeling Earth Systems* **11**, 4513–4558 (2019).